New Journal of Physics
The open-access journal for physics

Spectral shaping of laser generated proton beams

S M Pfotenhauer[1], O Jäckel[1], A Sachtleben[1], J Polz[1], W Ziegler[1], H-P Schlenvoigt[1], K-U Amthor[1], M C Kaluza[1], K W D Ledingham[2], R Sauerbrey[3], P Gibbon[4], A P L Robinson[5] and H Schwoerer[6]

[1] Institut für Optik und Quantenelektronik, Friedrich-Schiller-Universität Jena, Max-Wien-Platz 1, 07743 Jena, Germany
[2] Department of Physics, University of Strathclyde, Glasgow G4 0NG, UK
[3] Forschungszentrum Dresden-Rossendorf, POB 510119, 01314 Dresden, Germany
[4] John von Neumann Institute for Computing, ZAM, Forschungszentrum Jülich GmbH, 52425 Jülich, Germany
[5] Central Laser Facility, Rutherford-Appleton Laboratory, Chilton, Oxon, OX11 0QX, UK
[6] Laser Research Institute, University of Stellenbosch, Private Bag X1 7602 Matieland, South Africa
E-mail: pfotenhauer@ioq.uni-jena.de

New Journal of Physics **10** (2008) 033034 (14pp)
Received 3 January 2008
Published 27 March 2008
Online at http://www.njp.org/
doi:10.1088/1367-2630/10/3/033034

Abstract. The rapid progress in the field of laser particle acceleration has stimulated a debate about the promising perspectives of laser based ion beam sources. For a long time, the beams produced exhibited quasi-thermal spectra. Recent proof-of-principle experiments demonstrated that ion beams with narrow energy distribution can be generated from special target geometries. However, the achieved spectra were strongly limited in terms of monochromacity and reproducibility. We show that microstructured targets can be used to reliably produce protons with monoenergetic spectra above 2 MeV with less than 10% energy spread. Detailed investigations of the effects of laser ablation on the target resulted in a significant improvement of the reproducibility. Based on statistical analysis, we derive a scaling law between proton peak position and laser energy, underlining the suitability of this method for future applications. Both the quality of the spectra and the scaling law are well reproduced by numerical simulations.

Contents

1. Introduction

Throughout the past decade, high intensity lasers have ventured widely into the domain of particle acceleration [1, 2]. Current table-top laser systems of the 10 terawatt (TW) class readily generate ion beams of mega-electron-volt (MeV) energy [3]–[5] and bunches of relativistic electrons [6]–[8] by the interaction of ultraintense, ultrashort light pulses with matter. These particle beams possess a number of unique properties. They are initially very short pulsed, presumably comparable to the laser pulse duration [3]. Within this short time, they carry charges of pico- to nanocoulomb, which corresponds to currents exceeding 10^3 A. Moreover, laser accelerated protons show an excellent laminarity [9].

The proton acceleration process typically takes place on a micrometre scale, which has excited many speculations about the potential applications of such compact laser driven particle sources. However, most applications depend crucially on the availability of monoenergetic beams. Proposed schemes for the fast ignition of inertial confinement fusion with high energy particle pulses would benefit greatly from the availability of an intense, monoenergetic proton beam for the penetration of a pellet target [10]. The use of laser plasma sources as injectors [11] for conventional accelerators requires proton beams with small bandwidth and emittance in order to match the injected bunch to the subsequent conventional accelerator. And especially for cancer radiation therapy—as one of the most attractive applications—spectral control is an inevitable key criterion [1, 12]. However, hitherto laser produced proton beams commonly displayed a broad, quasi-thermal energy spectrum (see for example [3, 5, 13]), until in two recent proof-of-principle experiments laser accelerated ion beams with narrow-band spectra were achieved for the first time [14, 15].

Here, we present major advances in the laser production of monoenergetic proton beams. By improving substantially the microstructured targets first used in [15], it was possible to increase the quality of the resulting spectra both in terms of central peak energy and peak width. Importantly, an unprecedented reproducibility of $>80\%$ for the appearance of monoenergetic spectra was achieved after having investigated in detail the systematic removal of parasitic contamination layers on the target back side via laser ablation. This degree of reliability represents a vital improvement in comparison with the previous proof-of-principle experiments [14, 15]. Distinctly peaked spectra with approximately 10% bandwidth at 2 MeV were recorded for hundreds of laser shots. From this large number of spectra, a dependency of the average peak position on the laser pulse energy was deduced. The energy dependency is

summarized in an empirical scaling law, which is the first scaling law for monoenergetic spectra and deviates significantly from previous scalings obtained for the maximum proton energy of thermal spectra [3], [16]–[18]. The observed spectra and the scaling can be explained in terms of recent theoretical models and are strongly supported by two dimensional (2D) particle-in-cell (PIC) simulations.

2. Generation of monoenergetic proton beams from laser plasmas

When a high intensity laser pulse hits a thin metal foil, a hot plasma is formed at the target front side. In this plasma, electrons are accelerated by the laser field to relativistic energies and pushed into the target [19]. If the target is sufficiently thin, hot electrons are expelled at the back, where the restoring Coulomb force counteracts the charge separation. The main part of the hot electron population is trapped and constitutes an electron sheath behind the target [20, 21]. The sheath density scale length is that of a screened Coulomb potential in a free electron plasma, i.e. the Debye length $\lambda_D = (\varepsilon_0 k_B T_e/e^2 n_e)^{1/2}$, where T_e is the hot electron temperature and n_e the hot electron density behind the target. The resulting electric field between the sheath and the positively charged target is of the order of $10^{12}\,\mathrm{V\,m^{-1}}$ and suffices to field-ionize the foil material as well as contaminants present on the target surface (mainly hydrocarbons and water). The generated ions are accelerated immediately in the field, where the ions with the highest charge to mass (q/m) ratio, i.e. typically protons, are favoured for acceleration. This process is known as target normal sheath acceleration (TNSA) [21].

The proton beams produced show an exponential, quasi-thermal energy spectrum with a distinct cutoff energy $E_{\text{cut-off}}$ of typically a few MeV, which depends strongly on the laser and target parameters [13]. This broad distribution can be explained mainly by three contributions: first, the accelerating TNSA field is inhomogeneous in the transverse direction, which means that the maximum energy a proton can reach is determined by its radial position. Protons located in the centre of the field are accelerated the most, up to the maximum energy $E_{\text{cut-off}}$, whereas protons outside the centre experience a lower electric field strength and consequently are accelerated to lower energies. The inhomogeneous TNSA field distribution was measured with transverse probing of the electron density behind the foil, using proton deflectometry [22] or all optical probing set-ups [23], and exhibited a bell-shaped symmetry. This observation is in agreement with measurements of the beam divergence, which demonstrate that the proton emission takes place within symmetrical energy cones [9, 24]. A second contribution to the broad spectrum can be found in screening effects: as the electric field decays when reaching into regions of higher particle density, deeper sited protons in the source layer will be (partially) screened from the electric field by their faster predecessors. Both because of such screening effects as well as the transverse inhomogeneity, the resulting spectrum has a strong correlation to the initial distribution of the protons to be accelerated on the target. Thirdly, the acceleration process follows some intrinsic dynamics, which are correlated to the temporal profile of the incident laser pulse. While analytical models for proton acceleration sometimes refer to static parameters like an ‘effective acceleration time’ [3], numerical simulations show that the TNSA field actually takes some time to build up to its maximum field strength [25] so that the proton source is affected by different field strengths throughout the whole interaction.

Following this understanding, Esirkepov *et al* [26] proposed an acceleration scheme for the generation of monoenergetic proton beams, where all protons are radially confined to a ‘dot’ source within the central field region (figure 1). If the proton source is furthermore sufficiently

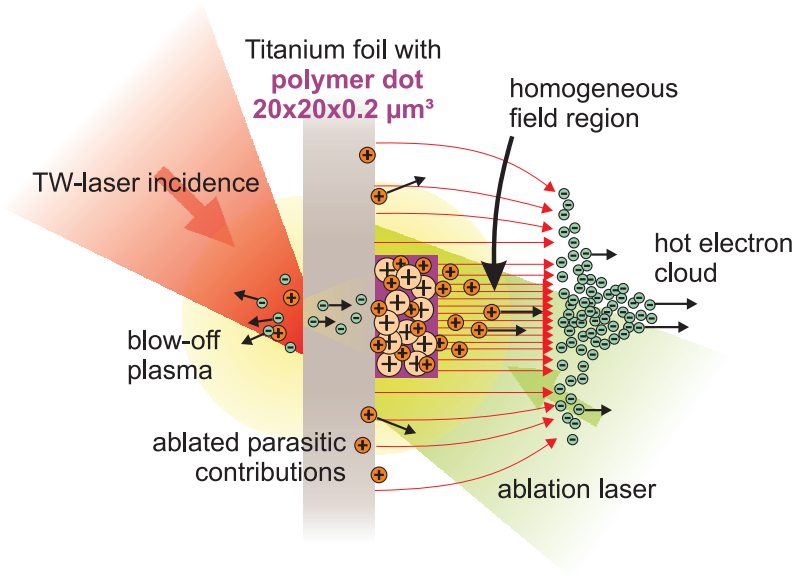

Figure 1. Confined TNSA from a micro-dot source. A TW-laser pulse hits a thin titanium foil at the front side exactly opposite to a polymer dot microstructure and creates a hot electron plasma. The electrons are accelerated in the laser field through the target and form a radially symmetric electron sheath at the back side, which gives rise to an electric of the order of a few TV m^{-1}. In this sheath field, surface atoms are ionized immediately and accelerated according to their charge to mass ratio up to MeV energies, whereas the light protons from the polymer dot outrun the heavier carbon ions and the titanium ions from the foil bulk. If a dot-like proton source is placed in the central part of the electron sheath field, protons from the dot will experience a uniform fraction of the transversely inhomogeneous field only [15, 26]. Numerical simulations show that the dot does not need to be as thin as possible (so as to avoid spectral broadening due to screening effects), but that the formation of monoenergetic spectra is caused by the low relative proton density in the polymer dot with respect to heavier ions. The additional charge separation between the protons and the different carbon charge states then creates a discontinuity in the charge density, which accelerates those protons close to the heavy ion front in a monoenergetic manner [27, 28]. In addition, one has to take care of parasitic proton contributions from surrounding contamination layers (e.g. oil or water vapour), which can be removed by controlled laser ablation of the target back side (cf below).

thin so that screening effects are negligible, all protons experience the same potential and are accelerated to a monoenergetic distribution. However, in a more recent theoretical study, Robinson and Gibbon [27] found that limiting the thickness of the proton layer is not a critical criterion: for thicker dots, the formation of monoenergetic spectra is supported by the charge separation between the light protons and more inert ions (e.g. carbon) at an early acceleration stage, where the slower ion front causes a discontinuity in the charge density and hence an electrostatic shock which accelerates protons like ‘test particles’ in front of a quasi-static

positive background. Similar charge separation arguments were involved in the explanation of the observed monoenergetic deuterons from droplet targets [29, 30], and spectral 'dips' as seen in [31]. Numerical simulations concerning micro-dot targets prove that this mechanism holds for robust dots of up to μm-thicknesses and may in fact vanish if the source layer is chosen too thin. The resulting proton spectrum thus has a strong dependency on the initial relative proton density in the source layer, and smaller relative proton densities may even lead to more pronounced monoenergetic spectra [27, 32]. The described radial confinement of the proton source was first realized by Schwoerer *et al*, where a proton rich dot was deposited on the target back side and located exactly opposite to the impact position of a TW laser pulse. Other approaches to monoenergetic ion beams include active spectral selection with laser driven micro-lenses [33, 34].

3. Target considerations and experimental set-up

The manufacturing of the microstructured targets for the proposed source confinement was realized in two steps. First, a layer of polymethyl methacrylate (PMMA) was applied on the back side of a 5 μm titanium foil using a spin coating technique ('double layer target') [35, 36]. In previous experiments, a typical increase in total proton number by a factor of 6 was observed for an extended PMMA layer of 500 nm thickness on a 5 μm titanium foil in comparison to an uncoated titanium foil [37]. In a second step, the coated target surface was microstructured with a femtosecond laser and a micrometre positioning system, where square dots of $20 \times 20\,\mu\text{m}^2$ were carved out of the PMMA surface. Alternatively, the microstructuring could be performed with an excimer laser through a lithographic mask, which yielded round dots of 10 μm diameter (figures 2b and (c)). From both types of targets, narrow band spectra were obtained consistently.

The experiments were carried out with the Jena 10 TW titanium : sapphire laser system (JETI), which delivered pulses of 800 mJ within 80 fs at a repetition rate of 10 Hz, focussed to a spot size of $A_{\text{FWHM}} = 5.5\,\text{m}^2$. With the help of a fast-switching Pockels cell a pulse contrast of $I_{\text{main}}/I_{\text{ASE}} > 10^8$ between the main laser pulse and the prior pedestal of amplified spontaneous emission (ASE) was attained 300 ps before the main pulse. The JETI laser pulse hit the thin foil target exactly opposite to the dot position (figure 2). For this purpose, the target back side was observed with a long distance microscope with micrometre resolution, and the JETI incidence position was marked on the observation screen such that the dots only needed to be translated to this reference position in order to achieve proper alignment. The overall accuracy of the alignment procedure could be estimated to about 5 μm.

In order to ensure the dots were the only proton source, a second laser was used to remove the parasitic hydrocarbon adsorption layers around the dots (cf figure 2). A frequency-doubled Nd : YAG ablation laser (532 nm, 5 ns pulse duration) hit the target back side under an angle of 22.5° co-centred with the JETI incidence position (figure 2). The laser was weakly focused on the target ($d_{\text{foc}}(1/e) \approx 600\,\mu\text{m}$) to cover the whole proton source area around the dot [38], and was attenuated with a variable set of density filters to apply well-defined ablation fluences.

In the experiment, the microstructured targets were irradiated with intensities of $I = 1\text{–}5 \times 10^{19}\,\text{W cm}^{-2}$, where the intensity was varied by changing the laser pulse energy. The generated proton and ion beams were limited by an aperture (0.3, 1 or 3 mm) and subsequently dispersed with a Thomson spectrometer (figure 2), whereas the aperture diameter defined the energy resolution of the detection set-up, e.g. $\Delta E_{\text{res}} = 50$ keV for 1 MeV protons with the 1 mm aperture. The particles were detected either with CR39 track detection plates or with an online

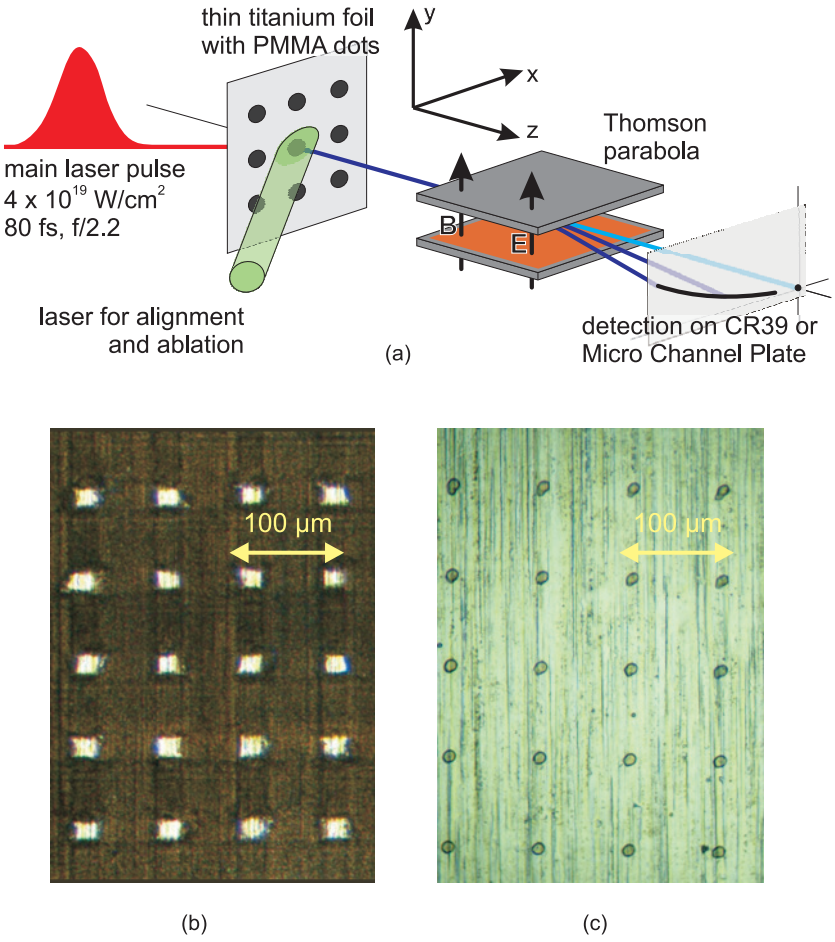

Figure 2. (a) Experimental set-up. The laser pulse hits the thin foil target at the front side exactly opposite to a micro-dot. Protons from the dot are accelerated within the central, homogeneous field region of the TNSA field and analysed with a Thomson spectrometer. The ions can be detected either with CR39 track detection plastics or an online imaging system (micro channel plate (MCP)). A second laser, which hits the target on the back side concentrically with respect to the first, is used for the cleaning of the target from residual contamination layer protons. (b) and (c) Microstructured target foils. (b) A 5 μm titanium foil carries polymer (PMMA) dots of 0.2 μm thickness, $20 \times 20\,\mu\text{m}^2$ extent and 80 μm separation. The dots were 'carved out' from a polymer layer with the help of a femtosecond laser system. (c) Lithography targets. Round dots of 0.2 μm thickness and 10 μm diameter with 80 μm separation were generated on the back side of a 5 μm titanium foil via lithography with a pulsed excimer laser. The second technique allows for a more flexible fabrication of micro-dots, which are, however, considerably more sensitive to laser ablation than those produced with the femtosecond system.

imaging system based on micro channel plates (MCPs). The use of an MCP allowed for a very flexible experimentation and facilitated the collection of large amounts of data. Since the MCP delivers only relative spectra, it was calibrated against both the absolute CR39 spectra and

at the TCC-CV28 cyclotron of the Physikalisch-Technische Bundesanstalt (German National Metrology Institute) in Braunschweig, Germany.

4. Results

4.1. Narrow-band proton spectra

Figure 3 shows a comparison between spectra obtained from shots on micro-dots of $20 \times 20 \times 0.2\,\mu\text{m}^3$ (dark grey and black line), and shots on a plain unstructured $5\,\mu$m titanium foil (black line). The black curve represents an average over six spectra and yields the typical smooth thermal distribution. In contrast, the dot spectra display distinct peak features, which are located at $E_{\text{center}} = 1.7\,\text{MeV}$ with $\Delta E_{\text{FWHM}} = 0.25\,\text{MeV} \approx 15\%$ energy width for shot #1 (dark grey line), and at $E_{\text{center}} = 2.5\,\text{MeV}$ with $\Delta E_{\text{FWHM}} = 0.2\,\text{MeV} \approx 8\%$ for shot #2 (black line). The relative peak contrast between the peak maximum and the low energy background is typically 10 within $2\Delta E_{\text{FWHM}}$ (i.e. $\approx 4000/400$ for shot #1 and $\approx 1000/100$ for shot #2). Shot #1 contains about 3×10^4 protons within $1\,\mu$Sr solid angle of observation, whereas the maximum exceeds the exponential distribution by a factor of 4. Conservative estimations based on beam divergence measurements at JETI and PIC simulations suggest that the full angle of emission of the narrow band protons is at least 24 mSr [15], which would yield a total number of $>10^9$ protons per shot in case of shot #1.

Drawing on the results from earlier numerical investigations [26, 27, 32], a 2D-PIC simulation was carried out for the micro-dot geometry, using the OSIRIS code [39]. The target consists of a dot, represented by a $0.2 \times 10\,\mu$m mixed slab of protons at $40\,n_{\text{crit}}$ ($m_{\text{p}}/m_{\text{e}} = 1830$) and heavy ions at $40\,n_{\text{crit}}(m_{\text{i}}/m_{\text{e}} = 3660)$, sitting on a $1.2\,\mu$m substrate slab containing only heavy ions ($m_{\text{i}}/m_{\text{e}} = 3660$) at a density of $80\,n_{\text{crit}}$. The laser pulse is normally incident at the centre of the foil. The temporal profile of the pulse is triangular, and it has a full width at half maximum (FWHM) duration of 80 fs. The simulation box is $20 \times 20\,\mu$m, and the cell sizes are $\Delta x = \Delta y = 2.5\,\text{nm}$. Initially, 64 particles were placed per species in each cell. The foil is initially centred in y, and the front surface of the foil is at $x = 5\,\mu$m. The simulations were run up to 350 fs.

Monoenergetic peaks appear consistently for a wide range of simulation parameters (e.g. varying focal spot size, pulse energy, simulation run time), if a micro-dot is irradiated. Figure 3(b) shows an exemplary spectrum obtained for $I = 2.7 \times 10^{19}\,\text{W cm}^{-2}$. A distinct peak is visible at 1.0 MeV, with 10% FWHM energy width and a contrast ratio of about 2 : 1, which is in good agreement with the experimental results. Since the formation of monoenergetic peaks strongly depends on the charge separation between different ion species, the slightly lower peak position can be attributed to the simplified resemblance of the dot composition, which contained only two ion species instead of multiple elements and ionization degrees, and the foil material, which was given by the dot heavy ion species instead of the heavier titanium, thus providing a smaller number of electrons.

Furthermore, it can be seen that the peak is not located at the cutoff energy of the proton spectrum, which continues with an exponential high energy tail. This behaviour can be explained as follows: besides the radial source confinement, the peak formation is affected by the electrostatic shock due to the charge separation between protons and carbons [28], whereas the protons that constitute the peak are those close to the ion front. As the heavy ion front is always slower than the fastest protons (lower q/m, screening effects), the central peak energy

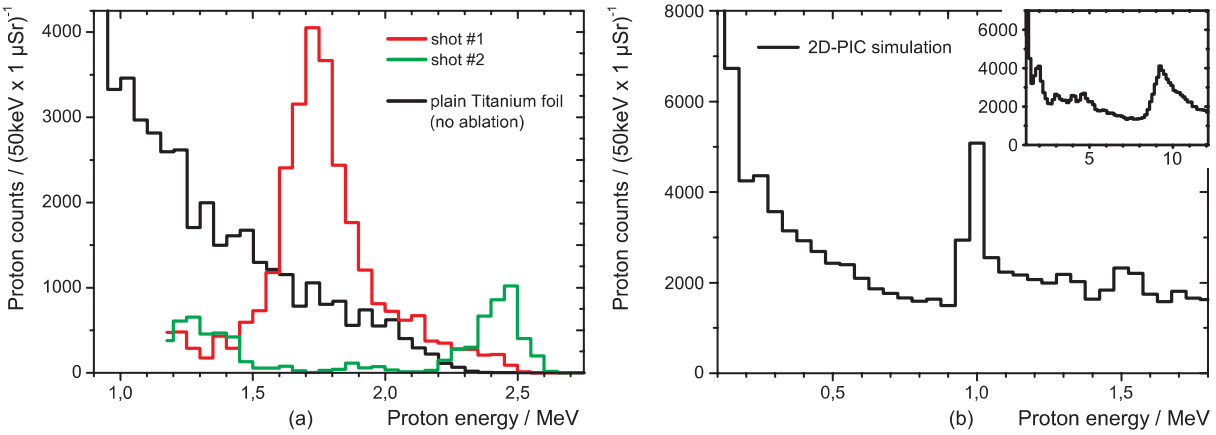

Figure 3. (a) Spectra from the irradiation of PMMA micro-dots ($20 \times 20 \times 0.2\,\mu\mathrm{m}^3$) after ten consecutive laser ablation shots at the threshold fluence of $\Phi_{\mathrm{abl}} = 1.2\,\mathrm{J\,cm^{-2}}$ (dark grey and black lines) in comparison to plain, unstructured $5\,\mu$m titanium foil (light grey line). The proton spectra from the polymer dots show distinct peaks at $E_{\mathrm{center}} = 1.7\,\mathrm{MeV}$ with an energy width of $\Delta E_{\mathrm{FWHM}} = 0.25\,\mathrm{MeV} = 15\%$ for shot #1 and $E_{\mathrm{center}} = 2.5\,\mathrm{MeV}$ with $\Delta E_{\mathrm{FWHM}} = 0.2\,\mathrm{MeV} = 8\%$ for shot #2. The ablation has suppressed the parasitic low-energy component of the spectrum and enables the acceleration of monoenergetic protons from the confined dot source. Narrow band features appear consistently once an ablation threshold fluence of $\Phi_{\mathrm{thr}} = 1.2\,\mathrm{J\,cm^{-2}}$ at 532 nm is surpassed. In contrast, the irradiation of a plain titanium foil (black line) yields the typical thermal distribution (average over 6 spectra). (b) Results of the 2D-PIC simulation carried out with the OSIRIS code. The interaction of a laser pulse with a $1\,\mu$m heavy ion foil carrying a micro-dot ($0.2\,\mu$m thickness, $10\,\mu$m radius) was simulated for an intensity of $I = 2.7 \times 10^{19}\,\mathrm{W\,cm^{-2}}$ (corresponding to $E_{\mathrm{laser}} = 0.5\,\mathrm{J}$ on target), whereas the dot consisted of 50% protons and 50% heavy ions. In good agreement with the experimental results, the calculated spectrum yields a distinct peak at 1.0 MeV with 10% bandwidth. The spectrum further possesses an exponential high energy tail, which indicates that the peak formation occurs at lower energy than the cutoff energy of corresponding thermal spectra. The inset of figure 3(b) shows the results of a simulation carried out for a laser pulse energy of 15 J. The obtained peak at 9.3 MeV underlines the suitability of the presented technique for future applications (cf also figure 5).

is necessarily below the maximum cutoff. This theoretical reasoning is in good agreement with experimental observations: monoenergetic peaks sometimes appear on top of an exponential background, and the detected peak positions are typically 30–50% lower in energy than the maximum achievable cutoff energy for thermal proton spectra obtained with the JETI laser. The separation between peak position and cutoff energy underlines that the reduced bandwidth is not merely a simple geometrical effect, but involves fundamentally different physics, which will be of importance when discussing the scalability of the effect to higher laser energies below.

4.2. Rear side ablation

Laser ablation can be used to clean the target surface from adsorbates and hence suppress the homogeneously distributed and hence unwanted regular TNSA proton source [40]. We first studied the impact of frequency-doubled Nd:YAG laser pulses ($\lambda = 532\,\mathrm{nm}$, $\tau_{\mathrm{pulse}} \approx 5\,\mathrm{ns}$) on plain titanium foils by varying the ablation fluence from $\Phi = 0.01$ to $10\,\mathrm{J\,cm^{-2}}$. Above a well-defined threshold fluence of $\Phi_{\mathrm{thr}} = (1.2 \pm 0.3)\,\mathrm{J\,cm^{-2}}$, the proton signal reduces to almost zero. The observed threshold corresponds to typical values for the ablation of organic layers from surfaces [41]. Below the threshold fluence, no ablation of contamination layers is expected, and indeed no effect on the proton acceleration could be identified.

In the next step, the effect of laser ablation was studied on microstructured targets. Below the threshold fluence, the observed proton beams correspond largely to those obtained from unstructured targets, i.e. they exhibit quasi-thermal spectra. However, once the threshold is surpassed, the continuous spectra are suppressed and distinct peak features appear (figure 3). We conclude that all contaminants have been eliminated; only the PMMA dot has resisted the ablation and remained as a confined proton source on the surface. Note that the ablation threshold of PMMA is about $3\,\mathrm{J\,cm^{-2}}$ at 308 nm [42], and should be even higher at 532 nm. In accordance with other results [40], the acceleration of titanium ions ($\mathrm{Ti^{1+}}$–$\mathrm{Ti^{4+}}$) from the foil bulk is observed when removing the contamination layer on the target back side, which agrees well with the estimated TNSA field strength of a few $10^{12}\,\mathrm{V\,m^{-1}}$.

Due to the vacuum conditions of the experiment, the ablated layers will start to recover immediately after the ablation has stopped. The timescale of such a recovery was studied by setting a delay between the last ablation shot and the JETI pulse. It turned out that after a delay of $\Delta t = 5\,\mathrm{s}$ the spectrum had regained its exponential form completely, which is, however, well above the 100 ms between two consecutive ablation shots. The recovery time of adsorption layers can be estimated by the particle impact rate on the surface $R = p/(3m\,k_{\mathrm{B}}T)^{1/2}$ [43], which follows directly from kinetic gas theory. Here, m is the mass of the adsorbed molecule and T the temperature in the target chamber. Assuming conservatively that the chamber pressure $p = 10^{-5}\,\mathrm{mbar}$ is determined by hydrocarbons only ($m_{\mathrm{CH4}} \approx 2.7 \times 10^{-25}\,\mathrm{kg}$), the impact rate at $T = 293\,\mathrm{K}$ attains $R = 6 \times 10^{15}\,\mathrm{cm^{-2}\,s^{-1}}$. A 12 Å contamination layer (as put forth in [44]) hence needs about 6 s to recover, in good agreement with our observations.

The ablation impact was also studied under single shot conditions. After one shot at the threshold fluence, almost all of the recorded spectra still display an exponential shape (figure 4). After two to four consecutive shots of ablation, the ratio between peaked and non-peaked spectra is evenly distributed, whereas for six or more shots the large majority of the spectra show a strongly reduced bandwidth. An irradiation with a higher fluence ($\Phi = 1.7\,\mathrm{J\,cm^{-2}} > \Phi_{\mathrm{thr}}$) reveals an even stronger dependence on the number of ablation shots. After two shots, 70% of the spectra are peaked, whereas after four shots almost all spectra show narrow-band features. This behaviour could be ascribed to initial incubation effects: the radiation induces defects in the contamination layer, which modifies the interatomic bonds and their coupling to the metal. The actual disposal of layers may thus not start immediately, but only after a critical number of defects have been accumulated [41]. However, with the help of controlled laser ablation, the generation of monoenergetic proton spectra from microstructured targets proves to be a highly reliable mechanism: an unprecedented reproducibility $>80\%$ was achieved over hundreds of shots, which represents a significant advance in laser proton acceleration.

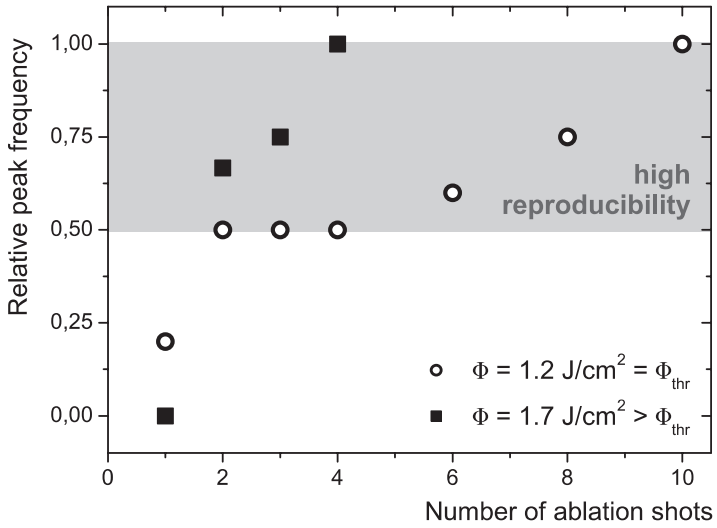

Figure 4. Relative frequency of peaked spectra as a function of the number of ablation shots. The back surface of the microstructured 5 μm titanium foil was ablated with a pulsed Nd:YAG laser ($\lambda = 532$ nm, $\tau_{\text{pulse}} = 5$ ns) in single shot mode, whereas the desorption of the surface contaminants is subject to initial incubation effects. After six consecutive ablation shots at the threshold fluence $\Phi_{\text{thr}} = 1.2\,\text{J cm}^{-2}$, 60% of the produced proton beams showed narrow-band spectra (whitened circles), which impressively demonstrates the reliability of the aiming and ablation procedure. For an increased fluence of $\Phi = 1.7\,\text{J cm}^{-2} > \Phi_{\text{thr}}$, an equally high reproducibility was reached after two shots already (black squares). In both cases, the relative frequency for the occurrence of peaked spectra approaches one when increasing the number of ablation shots. This means that narrow-band spectra are observed consistently, if a micro-dot is irradiated.

4.3. Energy scaling and future prospects

A subject of central interest for the generation of monoenergetic proton beams is the scalability of the technique to higher laser powers. We evaluated the peak position for many hundred spectra as a function of the JETI pulse energy while keeping all other parameters fixed. The use of an online detection system like an MCP facilitates the collection of such large amounts of data. It turned out that the average peak position increases from 1.42 to 1.63 MeV when the JETI pulse energy is increased from 0.5 to 0.8 J on target (figure 5, black squares). The four data points comprise a total of 140 spectra, all taken with 5 μm titanium foils carrying 200 nm thick dots, after ten consecutive shots of rear side ablation at the threshold fluence $\Phi_{\text{thr}} = (1.2 \pm 0.3)\,\text{J cm}^{-2}$. The energy range covered by the four data points was limited by the available laser energy and the range of the spectrometer. The error bars give the standard deviation of the sample sets and indicate the shot-to-shot fluctuation between the individual shots.

Various scaling laws have been proposed to connect the proton energy to the laser energy or intensity [16], [3]–[18]. All of these scalings refer to the cut-off energy of thermal spectra from plain foils, and it is known from previous measurements that the model by Fuchs *et al* [3] indeed

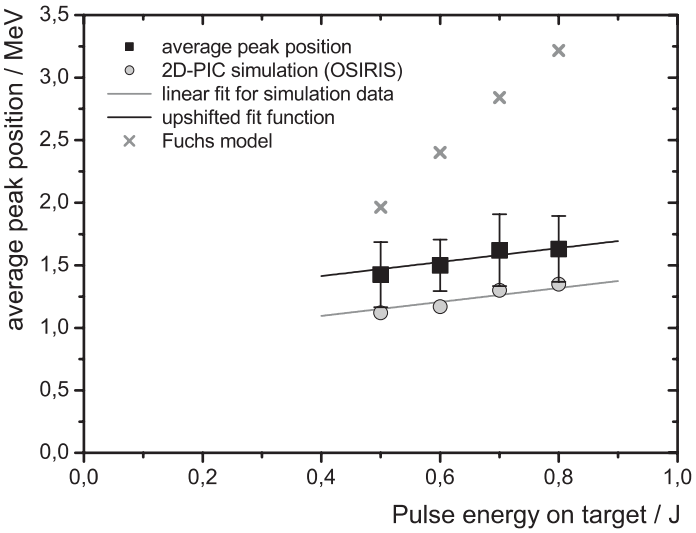

Figure 5. Energy dependency of monoenergetic proton peak position. The laser pulse energy on target was varied from 0.5 to 0.8 J, which corresponds to intensities of $2.9 - 4.7 \times 10^{19}\,\mathrm{W\,cm^{-2}}$. Consequently, the average peak position rose from 1.42 to 1.63 MeV (black squares). All other parameters were kept fixed (identical micro-dots on a 5 μm titanium foil; constant ablation conditions of ten consecutive shots at the threshold fluence). The four data points include a total of 140 monoenergetic spectra, which lends sufficient statistical significance to the results. The error bars represent the standard deviation of the statistical sample and thus delineate the shot-to-shot fluctuation. The observed proportionality is excellently reproduced by 2D-PIC simulations carried out for our experimental parameters (grey circles). The calculated peak positions lie slightly outside the standard deviation, but are well within statistical range of the sample sets. Together with an additional simulation for 15 J pulse energy (cf figure 3(b)), the calculated peak positions follow a linear function, $E_{\mathrm{peak}}^{\mathrm{scale}}/\mathrm{MeV} = 0.56 \times E_{\mathrm{laser}}/\mathrm{J} + 0.87$ (grey line), which represents the first scaling law particularly for monoenergetic spectra. All previous scaling laws refer to the cutoff energy of thermal spectra from plain foils and fail to account for our data. For example, the model by Fuchs *et al* [3] predicts much higher energies and a steeper slope (grey crosses) for the current parameters.

successfully predicts the observed cut-off energies at JETI. However, it has been shown above that the peak position does not coincide with the cutoff energy of the corresponding thermal spectrum, but is bound to the slower heavy ion front. Thus, the scaling laws cannot account for our peak positions. In fact, a comparison of our data with the scaling law from [3] shows a strong discrepancy for our narrow parameter interval already: the model by Fuchs *et al* predicts much higher energy values and an eight times steeper slope (grey crosses). We therefore conclude that cutoff energy scalings are inapplicable for the generation of monoenergetic spectra from microstructured targets.

In order to substantiate this conclusion, we extended our PIC simulation to the different laser energies applied in the analysis. The results are shown in figure 5 as grey

circles: when the laser energy is increased from 0.5 to 0.8 J, the calculated peak position shifts from 1.17 to 1.35 MeV. In agreement with the discussion of figure 3(b), the numerical results are systematically lower ($\Delta E \approx -300$ keV) than the experimental values. The calculated peak positions lie slightly outside the standard deviation, which still places them well into the statistical range of the sample sets.

The good accordance encouraged us to investigate the potential of micro-dot assisted proton acceleration for higher laser energies. An additional simulation was carried out for a pulse energy of 15 J, which is clearly in the range of the upcoming PW laser generation. The simulation yielded a monoenergetic peak at 9.3 MeV (inset figure 3(b)). In combination with the four calculated spectra between 0.5 and 0.8 J, the peak position was thus found to approximately follow a linear function $E_{\mathrm{peak}}^{\mathrm{scale}}/\mathrm{MeV} = 0.56 \times E_{\mathrm{laser}}/\mathrm{J} + 0.87$ (grey line in figure 5). It is striking how closely the slope of the simulation data matches that of the experimental data, as illustrated by the black line in figure 5 depicting the same linear fit function upshifted only by 320 keV. This accordance lends authority to the observed proportionality, which represents the first scaling law specifically for monoenergetic spectra.

Clearly, monoenergetic proton beams at 9.3 MeV central energy will not yet be a competitor for conventional accelerators. They will, however, be of great value when starting to investigate the suitability of laser accelerators as pre-acceleration stages for e.g. storage rings, which would be a first step to combine the unique acceleration fields of laser plasma sources with the mature conventional accelerator technology. Also, they will open up the possibility of the first biophysical experiments, such as pulsed proton irradiation of biological tissue. 10 MeV protons are capable of penetrating up to 1.2 mm into biological tissue, which—in conjunction with the narrow bandwidth—would allow for a concise dose application. For more conclusive estimations, the dependency of the peak properties on other laser parameters such as pulse duration and intensity has to be investigated, which will be the subject of future experiments. The continuation of the present work will also include the study of micro-dot targets both with reduced hydrogen concentration (as proposed in [27, 32]) as well as heavier dot materials (e.g. carbon dots). In the prospect of these promising experiments, however, today's capability of reliably generating 10^9 quasi-monoenergetic protons with less than 10% bandwidth by means of a scalable technique marks an important step towards application and will contribute significantly to the future of laser particle acceleration.

Acknowledgments

This work was funded by the Deutsche Forschungsgemeinschaft (DFG) within the transregional collaborative research center 'Relativistic Laser Plasma Dynamics' under contract TR18. We thank Burgard Beleites and Falk Ronneberger for their extensive support at JETI, as well as Waltraud Gräf and Dr Hans-Jörg Fuchs from the Institute of Applied Physics (IAP), Jena, for their help with the target fabrication. We also thank Volker Dangendorf, Roland Lauck, Kai Tittelmeier and the PTB Braunschweig for their support with the MCP calibration at the PTB cyclotron facility. SMP thanks Dr Nikita Arnold from the Johannes-Kepler-Universität Linz for his helpful comments on laser ablation, and the 'Evangelisches Studienwerk Villigst' for a long-term scholarship. APLR is grateful for the use of computing resources provided by Science and Technolgy Facilities Council's e-Science facility.

References

[1] Umstadter D 2001 Review of physics and applications of relativistic plasmas driven by ultra-intense lasers *Phys. Plasmas* **8** 1774–85

[2] Mourou G A, Tajima T and Bulanov S V 2006 Optics in the relativistic regime *Rev. Mod. Phys.* **78** 309–71

[3] Fuchs J *et al* 2006 Laser-driven proton scaling laws and new paths towards energy increase *Nat. Phys.* **2** 48–54

[4] Karsch S, Düsterer S, Schwoerer H, Ewald F, Habs D, Hegelich M, Pretzler G, Pukhov A, Witte K and Sauerbrey R 2003 High-intensity laser induced ion acceleration from heavy-water droplets *Phys. Rev. Lett.* **91** 015001

[5] Fritzler S, Malka V, Grillon G, Rousseau J P, Burgy F, Lefebvre E, d'Humieres E, McKenna P and Ledingham K W D 2003 Proton beams generated with high-intensity lasers: applications to medical isotope production *Appl. Phys. Lett.* **83** 3039–41

[6] Malka V *et al* 2002 Electron acceleration by a wake field forced by an intense ultrashort laser pulse *Science* **298** 1596–600

[7] Hidding B *et al* 2006 Generation of quasimonoenergetic electron bunches with 80-fs laser pulses *Phys. Rev. Lett.* **96** 105004

[8] Leemans W P, Nagler B, Gonsalves A J, Toth C, Nakamura K, Geddes C G R, Esarey E, Schroeder C B and Hooker S M 2006 GeV electron beams from a centimetre-scale accelerator *Nat. Phys.* **2** 696–9

[9] Cowan T E *et al* 2004 Ultralow emittance, multi-mev proton beams from a laser virtual-cathode plasma accelerator *Phys. Rev. Lett.* **92** 204801

[10] Roth M *et al* 2001 Fast ignition by intense laser-accelerated proton beams *Phys. Rev. Lett.* **86** 436–9

[11] Krushelnick K *et al* 2000 Ultrahigh-intensity laser-produced plasmas as a compact heavy ion injection source *IEEE Trans. Plasma Sci.* **28** 1184–9

[12] Bulanov S V and Khoroshkov V S 2002 Feasibility of using laser ion accelerators in proton therapy *Plasma Phys. Rep.* **28** 453–6

[13] Kaluza M, Schreiber J, Santala M I K, Tsakiris G D, Eidmann K, Meyer-ter Vehn J and Witte K J 2004 Influence of the laser prepulse on proton acceleration in thin-foil experiments *Phys. Rev. Lett.* **93** 045003

[14] Hegelich B M, Albright B J, Cobble J, Flippo K, Letzring S, Paffett M, Ruhl H, Schreiber J, Schulze R K and Fernandez J C 2006 Laser acceleration of quasi-monoenergetic mev ion beams *Nature* **439** 441–4

[15] Schwoerer H, Pfotenhauer S, Jäckel O, Amthor K U, Liesfeld B, Ziegler W, Sauerbrey R, Ledingham K W D and Esirkepov T 2006 Laser-plasma acceleration of quasi-monoenergetic protons from microstructured targets *Nature* **439** 445–8

[16] Mora P 2003 Plasma expansion into a vacuum *Phys. Rev. Lett.* **90** 185002

[17] Schreiber J *et al* 2006 Analytical model for ion acceleration by high-intensity laser pulses *Phys. Rev. Lett.* **97** 045005

[18] Robson L *et al* 2007 Scaling of proton acceleration driven by petawatt-laser-plasma interactions *Nat. Phys.* **3** 58–62

[19] Amiranoff F 2001 Fast electron production in ultra-short high-intensity laser-plasma interaction and its consequences *Meas. Sci. Technol.* **12** 1795–800

[20] Hatchett S P *et al* 2000 Electron, photon, and ion beams from the relativistic interaction of petawatt laser pulses with solid targets *Phys. Plasmas* **7** 2076–82

[21] Wilks S C, Langdon A B, Cowan T E, Roth M, Singh M, Hatchett S, Key M H, Pennington D, MacKinnon A and Snavely R A 2001 Energetic proton generation in ultra-intense laser-solid interactions *Phys. Plasmas* **8** 542–9

[22] Romagnani L *et al* 2005 Dynamics of electric fields driving the laser acceleration of multi-mev protons *Phys. Rev. Lett.* **95** 195001

[23] Polz J 2008 Zeitaufgelöste Untersuchung der Ionenbeschleunigung bei relativistischen Laser-Plasma-Wechselwirkungen an dünnen Folien *Master's Thesis* Friedrich-Schiller-University, Jena

[24] Snavely R A *et al* 2000 Intense high-energy proton beams from petawatt-laser irradiation of solids *Phys. Rev. Lett.* **85** 2945–8
[25] Velchev I, Fourkal E and Ma C M 2007 Laser-induced coulomb mirror effect: applications for proton acceleration *Phys. Plasmas* **14** 033106
[26] Esirkepov T Z *et al* 2002 Proposed double-layer target for the generation of high-quality laser-accelerated ion beams *Phys. Rev. Lett.* **89** 175003
[27] Robinson A P L and Gibbon P 2007 Production of proton beams with narrow-band energy spectra from laser-irradiated ultrathin foils *Phys. Rev.* E **75** 015401
[28] Robinson A P L, Bell A R and Kingham R J 2006 Fast electron transport and ionization in a target irradiated by a high power laser *Plasma Phys. Control. Fusion* **48** 1063–76
[29] Ter-Avetisyan S, Schnürer M, Nickles P V, Kalashnikov M, Risse E, Sokollik T, Sandner W, Andreev A and Tikhonchuk V 2006 Quasimonoenergetic deuteron bursts produced by ultraintense laser pulses *Phys. Rev. Lett.* **96** 145006
[30] Brantov A V, Tikhonchuk V T, Klimo O, Romanov D V, Ter-Avetisyan S, Schnürer M, Sokollik T and Nickles P V 2006 Quasi-mono-energetic ion acceleration from a homogeneous composite target by an intense laser pulse *Phys. Plasmas* **13** 122705
[31] Allen M *et al* 2003 Proton spectra from ultraintense laser-plasma interaction with thin foils: experiments, theory, and simulation *Phys. Plasmas* **10** 3283–9
[32] Robinson A P L, Bell A R and Kingham R J 2006 Effect of target composition on proton energy spectra in ultraintense laser-solid interactions *Phys. Rev. Lett.* **96** 035005
[33] Toncian T *et al* 2006 Ultrafast laser-driven microlens to focus and energy-select mega-electron volt protons *Science* **312** 410–3
[34] Willi O *et al* 2007 Laser triggered micro-lens for focusing and energy selection of MeV protons *Laser Part. Beams* **25** 71–7
[35] Badziak J, Woryna E, Parys R, Platonov K Y, Jablonski S, Rye L, Vankov A B and Wolowski J 2001 Fast proton generation from ultrashort laser pulse interaction with double-layer foil targets *Phys. Rev. Lett.* **8721** 215001
[36] Roth M *et al* 2002 Energetic ions generated by laser pulses: a detailed study on target properties *Phys. Rev. ST—Accelerators Beams* **5** 061301
[37] Jäckel O 2006 Vermessung von Ionenspoktren aus relativistischen laserproduzierten Plasmen *Master's Thesis* Friedrich-Schiller-University, Jena
[38] Schreiber J *et al* 2004 Source-size measurements and charge distributions of ions accelerated from thin foils irradiated by high-intensity laser pulses *Appl. Phys.* B **79** 1041–5
[39] Lee S, Katsouleas T, Hemker R and Mori W B 2000 Simulations of a meter-long plasma wakefield accelerator *Phys. Rev.* E **61** 7014–21
[40] Hegelich M *et al* 2002 MeV ion jets from short-pulse-laser interaction with thin foils *Phys. Rev. Lett.* **89** 085002
[41] Bäuerle D 1996 *Laser Processing and Chemistry* (Berlin: Springer)
[42] Costela A, Figuera J M, Florido F, Garciamoreno I, Collar E P and Sastre R 1995 Ablation of poly(methyl methacrylate) and poly(2-hydroxyethyl methacrylate) by 308-nm, 222-nm and 193-nm excimer-laser ablation *Appl. Phys.* A **60** 261–70
[43] Zangwill A 1988 *Physics at Surfaces* (Cambridge: Cambridge University Press)
[44] Allen M, Patel P K, Mackinnon A, Price D, Wilks S and Morse E 2004 Direct experimental evidence of back-surface ion acceleration from laser-irradiated gold foils *Phys. Rev. Lett.* **93** 265004